Optics Communications 384 (2017) 1–6

Contents lists available at ScienceDirect

Optics Communications

journal homepage: www.elsevier.com/locate/optcom

Photonic generation of versatile frequency-doubled microwave waveforms via a dual-polarization modulator

Zihang Zhu*, Shanghong Zhao, Xuan Li, Kun Qu, Tao Lin

School of Information and Navigation, Air Force Engineering University, Xi'an 710077, China

ARTICLE INFO

Keywords:
Triangular waveform generation
Square waveform generation
Dual-polarization modulator

ABSTRACT

We report a photonic approach to generate frequency-doubled microwave waveforms using an integrated electro-optic dual-polarization modulator driven by a sinusoidal radio frequency (RF) signal. With active bias control, two MZMs of the dual-polarization modulator operate at minimum transmission points, a triangular waveform can be generated by a parameter setting of modulation index. After introducing a broadband 90° microwave phase shifter, a square waveform can be obtained by readjusting the power relationship of harmonics. The proposal is first theoretically analyzed and then validated by simulation. Simulation results show that a 10 GHz triangular and square waveform sequences are successfully generated from a 5 GHz sinusoidal RF drive signal, and the performance of the microwave waveforms are not influenced by the finite extinction ratio of modulator.

1. Introduction

Photonic generation of microwave waveform has attracted much attention due to its wide applications in modern radar systems, wired and wireless communications, and all-optical microwave signal processing and manipulation [1–5]. Compared with the electrical techniques, which generate the microwave waveforms with the bandwidth limited to below 20 GHz, photonic generation of microwave waveforms has the advantages of wide bandwidth, large frequency tunable range, low loss, and immunity to electromagnetic interference. In recent years, various optical approaches have been reported to generate microwave waveform such as optical spectral shaping [6,7], frequency to time mapping [8], external modulation [9–14] and so on. Among them, the external modulation of a continuous wave (CW) optical signal exhibits the merits of low cost and high flexibility in wave shape.

The principle for microwave waveform generation using external modulation is based on controlling the phases and amplitudes of the optical sidebands generated due to the nonlinearity of the external modulator. It was reported that triangular waveform can be generated using a Mach–Zehnder modulator (MZM) combined with a dispersive element [9,10]. However, the repetition rate of the generated waveform is difficult to tune due to the use of fiber. In [11], a method to generate triangular waveforms using a MZM biased at the minimum transmission point and stimulated Brillouin scattering (SBS) in optical fiber was proposed. However, the SBS effect is sensitive to the environmental fluctuations, which may make the system unstable. In [12,13], triangular waveforms were generated using a dual-parallel MZM (DPMZM) in conjunction with a 90° electrical hybrid coupler or a tunable optical bandpass filter. However, the repetition frequency of the generated waveform equals to the frequency of RF drive signal, which is restricted by the bandwidth of modulator and electrical devices. In order to improve the frequency multiplication factor, a frequency-doubled triangular waveform was generated using a DPMZM combined with a frequency tripler [14]. Since the undesired optical sidebands are suppressed by controlling three bias points of DPMZM, the finite extinction ratio has an impact or distortion on the final waveform. Although the major distortion can be removed by bias control, the shape of the generated triangular waveform may be deteriorated when the extinction ratio is lower than 25 dB.

In this paper, we propose a versatile frequency-doubled microwave waveforms generation method based on a commercially available integrated dual-polarization modulator. By properly choosing the system parameters including the modulation index and the direct current bias phase shift, frequency-doubled triangular and square waveform sequences with a full duty cycle can be generated. A theoretical analysis leading to the operating conditions to obtain triangular and square waveforms is developed and demonstrated by simulation. Besides, the effects of several non-ideal factors on the performance of the microwave waveforms are analyzed. Simulation results show that the finite extinction ratio has no impact on the waveform.

* Corresponding author.
E-mail address: zhuzihang6@126.com (Z. Zhu).

http://dx.doi.org/10.1016/j.optcom.2016.10.015
Received 8 September 2016; Received in revised form 3 October 2016; Accepted 8 October 2016
Available online 13 October 2016

2. Principle

The schematic diagram of the proposed frequency-doubled microwave waveform generation scheme is shown in Fig. 1. A light wave from a laser diode (LD) is sent to a dual-polarization modulator via a polarization controller (PC). The dual-polarization modulator is a commercially available integrated device (FUJITSU FTM7980EDA) including a polarization beam splitter (PBS), a polarization beam combiner (PBC), and two MZMs. In the real system, the length of two paths are different, which leads to the phase imbalance between two radio frequency drive signals applied to two MZMs. In order to solve this problem, two tunable electrical phase shifters should be connected in the two paths to adjust the phase of two radio frequency drive signals. A low-frequency microwave signal is divided into two paths and applied to the two MZMs. By adjusting PC to let the polarization state of the input light wave an angle of 45° to one principal axis of the PBS, the output of the MZM1 can be expressed as.

$$E_x(t) = \frac{\sqrt{2}}{2} E_c e^{jw_c t}\left[\gamma_1 e^{jm_1 \sin(w_m t+\theta)} + (1-\gamma_1) e^{j\varphi_1} e^{-jm_1 \sin(w_m t+\theta)}\right] \tag{1}$$

where E_c and w_c are the amplitude and angular frequency of the optical carrier, w_m and θ are the angular frequency and initial phase of the input microwave signal, m_1 is the modulation index of the MZM1, $\gamma_1 = (1 - 1/\sqrt{\varepsilon_{r1}})/2$ is the power splinting or combining ration of arm two for the Y-branch waveguide of MZM1, ε_{r1} is the extinction ratio, and φ_1 is the direct current bias phase shift of MZM1.

Microwave driving signals of MZM1 and MZM2 are from the same RF signal. The difference is that a frequency tripler (FT) is used in the lower path, resulting in a frequency triple of the driving signal. Thus, the output of the MZM2 can be expressed as

$$E_y(t) = \frac{\sqrt{2}}{2} E_c e^{jw_c t}\left[\gamma_2 e^{jm_2 \sin(3w_m t+3\theta)} + (1-\gamma_2) e^{j\varphi_2} e^{-jm_2 \sin(3w_m t+3\theta)}\right] \tag{2}$$

where m_2 is the modulation index of the MZM2, $\gamma_2 = (1 - 1/\sqrt{\varepsilon_{r2}})/2$ is the power splinting or combining ration of arm two for the Y-branch waveguide of MZM2, ε_{r2} is the extinction ratio, and φ_2 is the direct current bias phase shift of MZM2.

Then, the output of MZM1 and MZM2 are combined by the PBC. After amplified by an erbium-doped fiber amplifier (EDFA) and detected by a square-law PD, the photocurrent can be expressed as

$$\begin{aligned} I(t) &= RG(|E_x(t)|^2 + |E_y(t)|^2) \\ &= \frac{RGE_c^2}{2}\{\gamma_1^2 + (1-\gamma_1)^2 + 2\gamma_1(1-\gamma_1)\cos[2m_1 \sin(w_m t+\theta) - \varphi_1] \\ &\quad + \gamma_2^2 + (1-\gamma_2)^2 + 2\gamma_2(1-\gamma_2) \\ &\quad \cos[2m_2 \sin(3w_m t+3\theta) - \varphi_2]\} \end{aligned} \tag{3}$$

where R is the PD responsivity, and G is the EDFA gain.

If the MZM1 and MZM2 are biased at the minimum transmission points (φ_1=φ_2=π), using Jacobi–Anger expansion, the photocurrent can be rewritten as

$$\begin{aligned} I(t) = \frac{RGE_c^2}{2}\{&\gamma_1^2 + (1-\gamma_1)^2 - 2\gamma_1(1-\gamma_1)\{J_0(2m_1) + 2\textstyle\sum_{n=1}^{\infty} J_{2n}(2m_1)\cos[2n(w_m t+\theta)]\} \\ &+\gamma_2^2 + (1-\gamma_2)^2 - 2\gamma_2(1-\gamma_2)\{J_0(2m_2) + 2\textstyle\sum_{n=1}^{\infty} J_{2n}(2m_2) \\ &\cos[2n(3w_m t+3\theta)]\}\} \end{aligned} \tag{4}$$

where J_n is the (n)th-order Bessel function of the first kind. It can be seen from Eq. (4) that only even-order harmonics are generated. We consider only frequency components up to second-harmonic, which means the modulation indices should be adjusted to relatively small value ($m_1 < 1$ and $m_2 < 1$). Eq. (4) becomes

$$\begin{aligned} I(t) = \frac{RGE_c^2}{2}\{&\gamma_1^2 + (1-\gamma_1)^2 - 2\gamma_1(1-\gamma_1)[J_0(2m_1) + 2J_2(2m_1)\cos(2w_m t+2\theta)] \\ &+\gamma_2^2 + (1-\gamma_2)^2 - 2\gamma_2(1-\gamma_2)[J_0(2m_2) + 2J_2(2m_2)\cos(6w_m t+6\theta)]\} \end{aligned} \tag{5}$$

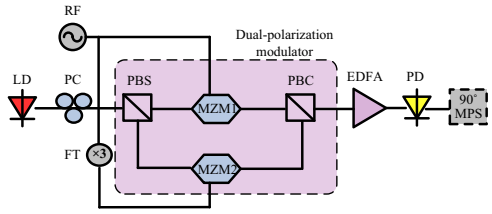

Fig. 1. Schematic diagram of a frequency-doubled microwave waveform generation system using a dual-polarization modulator. LD: laser diode; PC: polarization controller; PBS: polarization beam splitter; MZM: Mach–Zehnder modulator; PBC: polarization beam combiner; EDFA: erbium-doped fiber amplifier; PD: photodetector; RF: radio frequency; FT: frequency tripler; MPS: microwave phase shifter.

2.1. Triangular waveform

It is known that the Fourier series expansion of a triangular waveform can be expressed as

$$T_{tr}(t+t_0) = A_{tr} + B_{tr}\sum_{k=1,3,5}^{\infty}\frac{1}{k^2}\cos(k\Omega t + k\Omega t_0) \tag{6}$$

where A_{tr} and B_{tr} represent constant value, Ω is the fundamental angular frequency, t_0 is constant time. Eq. (6) shows that the shape of a triangular waveform is unchanged if phase shift $k\Omega t_0$ (k=1, 3, 5...) is introduced to the harmonic of the triangular waveform. Eq. (6) can not be satisfied for every k, an ideal triangular-shaped waveform is not feasible. However, a triangular waveform can be approximated by a finite number of the Fourier series components [15,16]. The triangular waveforms with and without considering fifth-order harmonic are simulated numerically, as shown in Fig. 2. It can be seen from Fig. 2 that the triangular waveforms with and without fifth-order harmonic are almost the same since the fifth-order harmonic is with very small amplitude and can not make a significant contribution to the final waveform. Thus, in our case, two Fourier components will be considered, and the modulation indices should be adjusted to meet the following relationship:

$$\gamma_1(1-\gamma_1)J_2(2m_1) = 9\gamma_2(1-\gamma_2)J_2(2m_2) \tag{7}$$

Eq. (5) can be rewritten as

$$I_{tr}(t) = A + B\left[\cos(\Omega t + \Omega t_0) + \frac{1}{9}\cos(3\Omega t + 3\Omega t_0)\right] \tag{8}$$

where

$$\begin{aligned} A = \frac{RGE_c^2}{2}\{&\gamma_1^2 + (1-\gamma_1)^2 - 2\gamma_1(1-\gamma_1)J_0(2m_1) + \gamma_2^2 + (1-\gamma_2)^2 \\ &- 2\gamma_2(1-\gamma_2)J_0(2m_2)\} \end{aligned} \tag{9}$$

$$B = -2RGE_c^2\gamma_1(1-\gamma_1)J_2(2m_1) \tag{10}$$

$$\Omega = 2w_m, \text{ and } \Omega t_0 = 2\theta$$

2.2. Square waveform

It is known that the Fourier series expansion of a square waveform can be expressed as

$$T_{sq}(t+t_0) = A_{sq} + B_{sq}\sum_{k=1,3,5}^{\infty}\frac{1}{(-1)^{\frac{k-1}{2}}k}\cos(k\Omega t + k\Omega t_0) \tag{11}$$

Similar to the triangular waveform, Eq. (11) can not be satisfied for every k, an ideal square waveform is not feasible. The square waveforms with and without considering fifth-order harmonic are simulated numerically, as shown in Fig. 3. In can be seen from Fig. 3 that the influence of the higher order harmonic on the waveform quality of the square waveform is obvious. Compared with the generation of a triangular waveform, the generation of a square waveform needs more

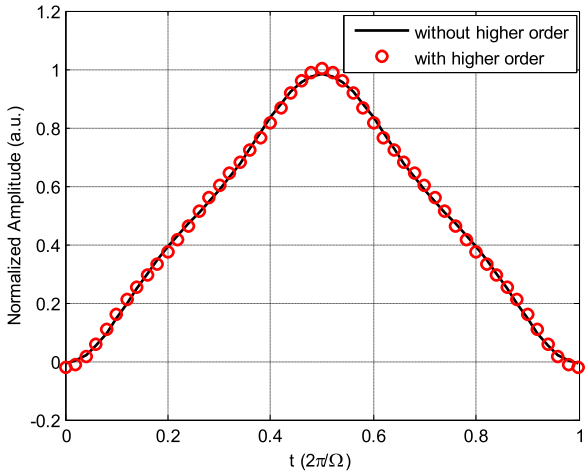

Fig. 2. Numerical result of triangular waveform.

Fourier series components to approach the ideal shape. Besides, the influence of the higher order harmonic on the power efficiency of the square waveform is small. In our paper, considering the limited input microwave power in the real applications, we only consider two Fourier series components [15]. Thus, the modulation indices should be adjusted to meet the following relationship:

$$\gamma_1(1-\gamma_1)J_2(2m_1) = 3\gamma_2(1-\gamma_2)J_2(2m_2) \tag{12}$$

In this case, Eq. (5) can be rewritten as

$$I(t) = A + B\left[\cos(\Omega t + \Omega t_0) + \frac{1}{3}\cos(3\Omega t + 3\Omega t_0)\right] \tag{13}$$

It can be seen from Eq. (13) that the phase relation for the fundamental tone and the third-order harmonic violates the requirement for generation of a square waveform (see Eq. (11)). If a broadband 90° microwave phase shifter is attached after the PD to introduce a 90° phase shift to both the fundamental tone and the third-order harmonic, Eq. (13) is rewritten as

$$I_{sq}(t) = A + B\left[\cos(\Omega t + \Omega t_0 + \frac{\pi}{2}) - \frac{1}{3}\cos(3\Omega t + 3\Omega t_0 + \frac{3\pi}{2})\right] \tag{14}$$

It is apparent that Eq. (14) fully meets the requirement for generation of a square waveform as shown in Eq. (11).

3. Simulation results and discussion

In order to verify the quality of the generated triangular waveform and square waveform signals, a simulation system is set up based on the OptiSystem platform as shown in Fig. 1. The laser operates at a wavelength of 1552.5 nm (193.1 THz), linewidth of 10 MHz and power of 10 dBm. The two MZMs with the extinction ratios of 30 dB are biased at the minimum transmission points, which are connected by a PBS and a PBC in parallel. In the real system, the direct current bias drift of two MZMs may happen in several seconds, which makes the system unstable. In order to solve this problem, a sophisticated control circuit is needed to stabilize the operation. The frequency of the RF drive signals are set at 5 GHz and 15 GHz. An erbium-doped fiber amplifier (EDFA) with gain of 20 dB and noise figure of 4 dB is utilized to compensate for the insertion loss of the modulator. The responsivity of PD is 0.8 A/W, dark current is 10 nA, and the thermal noise is 1×10^{-22} W/Hz. The electrical signal is measured by a spectrum analyzer and an oscilloscope. In order to generate a triangular waveform, the modulation indices of two MZMs are adjusted to 0.49 and 0.16 according to Eq. (7). In order to generate a square waveform, a broadband 90° microwave phase shifter is added after the PD and the modulation indices of two MZMs are adjusted to 0.49 and 0.28 according to Eq. (12). However, it is difficult to obtain the accurate modulation index in the real system by adjusting the power of the radio frequency drive signal to its desired value since the precision of the electrical tunable attenuator is limited.

First, the performance of triangular waveform is investigated. The simulated electrical spectrum of triangular waveform is shown in Fig. 4(a), which mainly consists of the second-order harmonic at 10 GHz and the sixth-order harmonic at 30 GHz. The sixth-order harmonic is 19.1 dB lower than the second-order one, which agrees well with the theoretical value shown in Eq. (8). Besides, the undesired fourth-order harmonic signal is well suppressed and is 34 dB lower than the second-order harmonic. The simulated triangular waveform is shown in Fig. 4(b). As can be seen, a triangular waveform with the repetition rate of 10 GHz is successfully generated, which is two times frequency of the RF drive signal.

In practice, extinction ratio of a commercially available MZM may be lower than 30 dB, and the extinction ratios of two MZMs may be different. Thus, it is necessary to investigate the impact of non-ideal extinction ratio on the performance of the generated triangular waveform. The simulated electrical spectrum with 20 dB extinction ratio of MZM1 and 30 dB extinction ratio of MZM2 is shown in Fig. 5(a). It can be seen from Fig. 5(a) that the sixth-order harmonic is 19 dB lower than the second-order one, and the undesired fourth-order harmonic signal is also well suppressed. Thus, a 10 GHz triangular waveform is also successfully generated, as shown in Fig. 5(b).

The simulated electrical spectrum and triangular waveform with 20 dB extinction ratios of two MZMs are shown in Fig. 6. It can be seen from Fig. 6 that a 10 GHz triangular waveform with a little higher amplitude than the triangular waveforms generated in Figs. 4 and 5 is obtained. This is due to the influence of extinction ratio on the direct current component of the triangular waveform. However, the shape of the triangular waveform is almost unchanged, since the power ratio between sixth-order harmonic and second-order one is not affected by the variation of extinction ratio. Thus, the impact of non-ideal extinction ratio on the performance of the generated triangular waveform can be ignored. While for the DPMZM scheme proposed in [14], obvious power fading exists with the same extinction ratios.

The impact of MZM1 bias drift on the performance of the generated triangular waveform is also investigated. Fig. 7(a) shows the triangular waveform when the bias voltage deviation ratio of MZM1 is 5%. The bias voltage deviation ratio is defined as $(\Delta V/V_\pi)\times100\%$, where ΔV is bias voltage deviation and V_π is the half-wave voltage of the MZM. It can be seen from Fig. 7 that power fading exists and the fading period can be figured out as 200 ps. To solve such a problem, the bias phase shift of MZM2 (φ_2) is switched from 180° to 183.2°. In this case, a 10 GHz triangular waveform with less distortion and steady-state

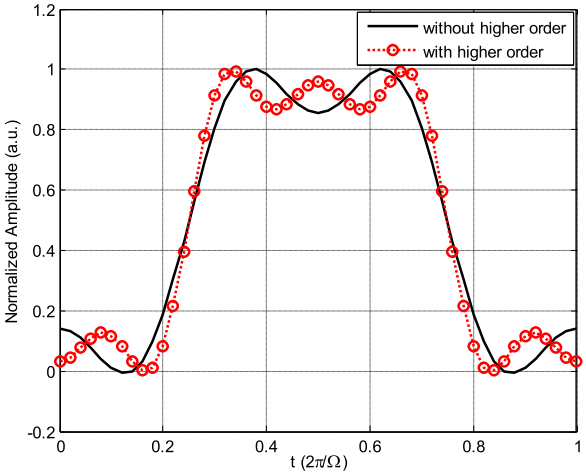

Fig. 3. Numerical result of square waveform.

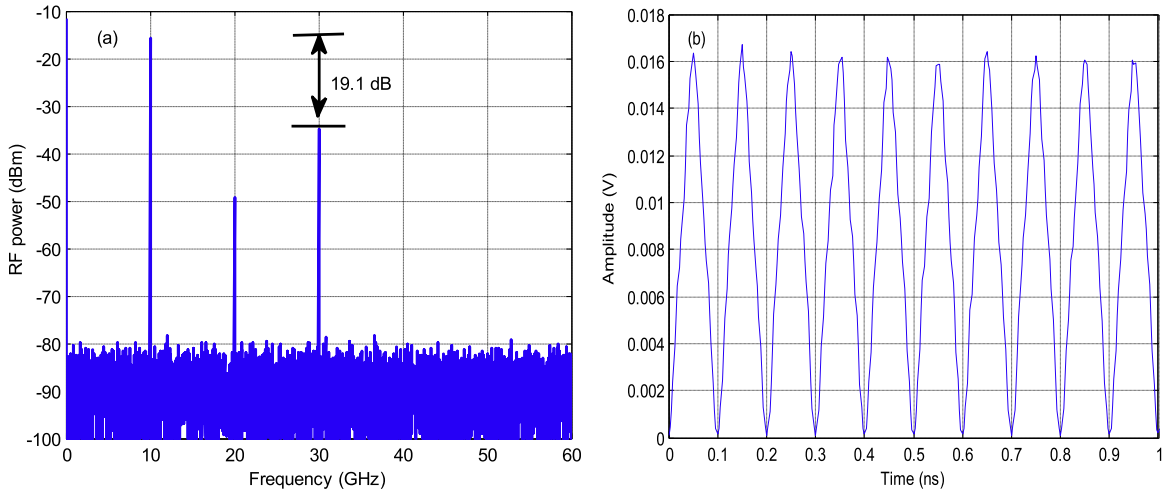

Fig. 4. Generation of frequency-doubled triangular waveform when the extinction ratios of two MZMs are 30 dB. (a) The simulated electrical spectrum of the 10 GHz triangular waveform. (b) The simulated 10 GHz triangular waveform.

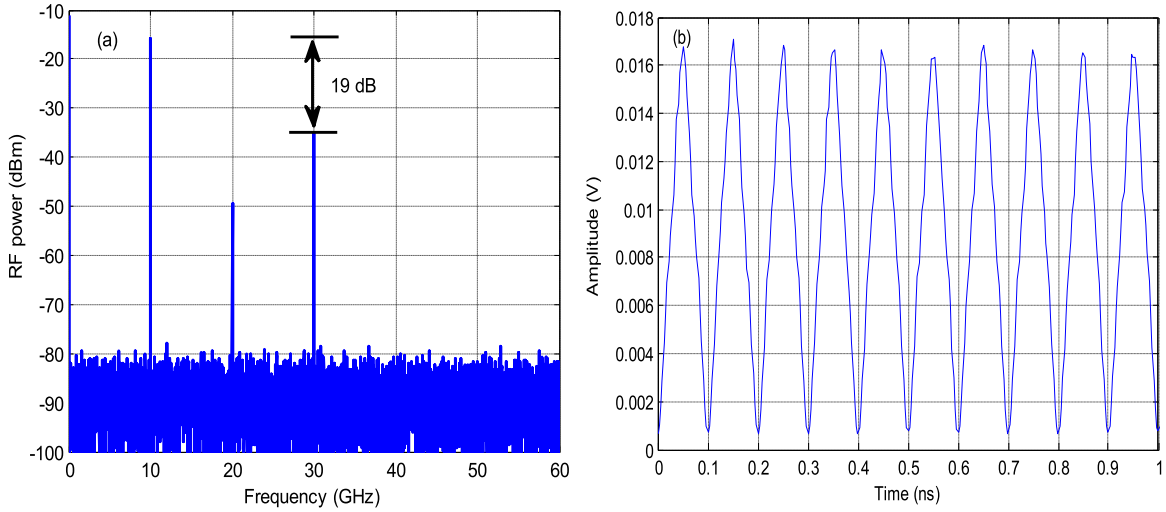

Fig. 5. Generation of frequency-doubled triangular waveform when the extinction ratio of MZM1 is 20 dB and the extinction ratio of MZM2 is 30 dB. (a) The simulated electrical spectrum of the 10 GHz triangular waveform. (b) The simulated 10 GHz triangular waveform.

power is generated, as shown in Fig. 7(b). Thus, the impact of MZM1 bias drift on the performance of the generated triangular waveform can be alleviated by controlling the bias phase shift of MZM2.

Next, we will show that the proposed microwave waveform generator is also capable of generating square waveform. The simulated electrical spectrum of square waveform is shown in Fig. 8(a). The undesired fourth-order harmonic is 33 dB lower than the second-order one. Thus, the contribution of the fourth-order harmonic can be ignored. The desired sixth-order harmonic is 9.5 dB lower than the second-order one. This value is very close to the theoretical one calculated in Eq. (14). The simulated square waveform is shown in Fig. 8(b). It can be seen that a square waveform with repetition rate two times frequency of the RF drive signal is successfully generated.

Besides, the impact of non-ideal extinction ratio on the performance of the generated square waveform are also investigated, as shown in Figs. 9 and 10. It can be seen that the shape of the square waveform is almost unchanged, since the power ratio between sixth-order harmonic and second-order one is not affected by the variation of extinction ratio. Thus, the impact of non-ideal extinction ratio on the performance of the generated square waveform can be neglected.

4. Conclusion

We have demonstrated a photonic frequency-doubled microwave waveforms generator based on a dual-polarization modulator driven by a sinusoidal RF signal. The desired microwave waveform can be generated by properly choosing the system parameters including the modulation index, the direct current bias phase shift, and the phase of electrical harmonics. A theoretical analysis is developed, which is validated by a simulation. A triangular and a square waveform with a repetition rate of 10 GHz can be generated from a 5 GHz sinusoidal RF drive signal. Besides, the effects of several non-ideal factors on the performance of the microwave waveforms are analyzed. Compared with the microwave waveform generated using a DPMZM, the performance of the generated triangular and square waveform using a dual polarization modulator are not affected by the extinction ratio of the modulator. Even if the extinction ratios of two MZMs are lower than 30 dB or they are different, the shape of the generated waveform is unchanged. For the triangular waveform, when the bias drift of one MZM happens, the major distortion can be removed by controlling the bias of the other MZM.

Acknowledgment

This research was supported by the National Natural Science Foundation of China (Nos. 61401502 and 61571461) and the Natural Science Foundation of Shaanxi Province (No. 2016JQ6008).

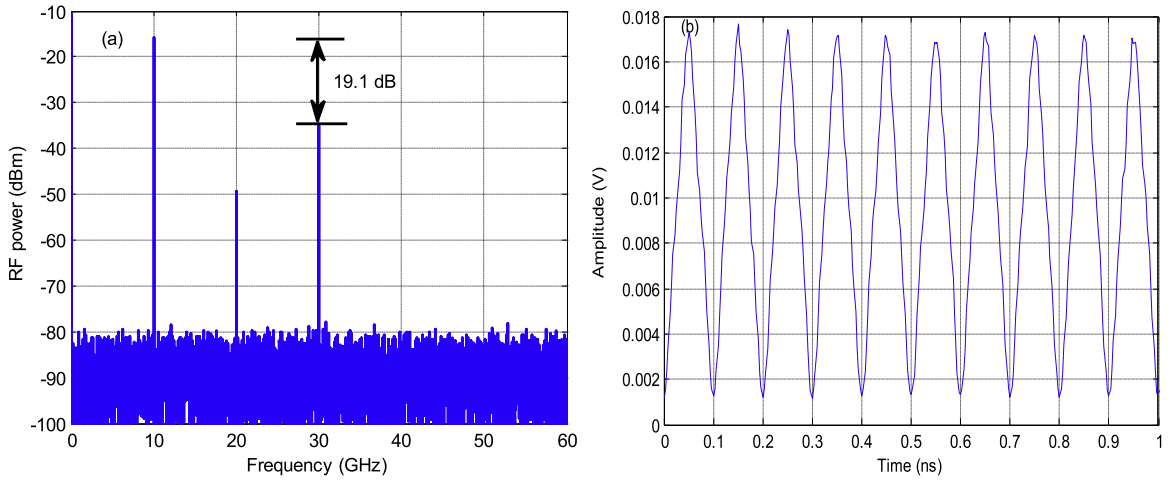

Fig. 6. Generation of frequency-doubled triangular waveform when the extinction ratios of two MZMs are 20 dB. (a) The simulated electrical spectrum of the 10 GHz triangular waveform. (b) The simulated 10 GHz triangular waveform.

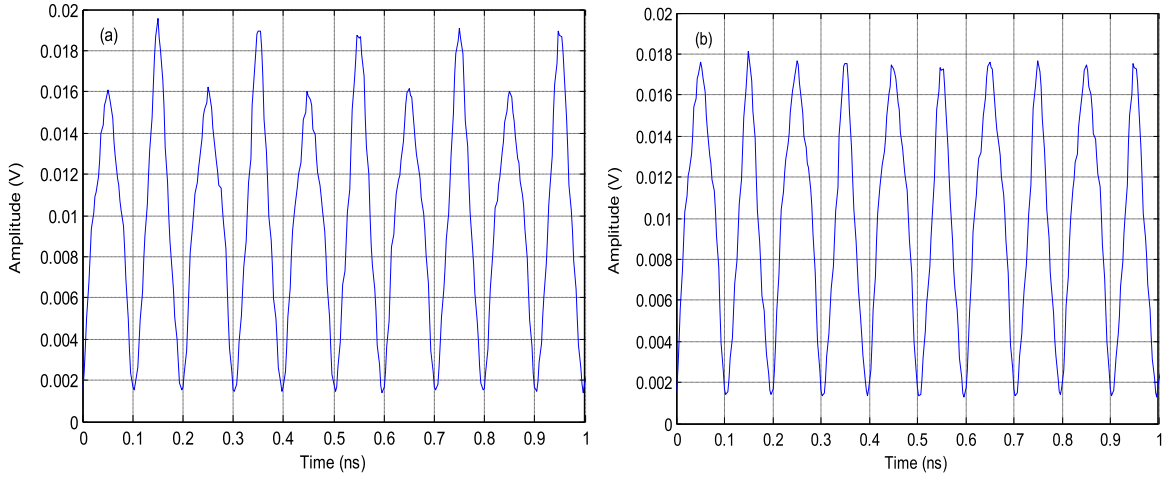

Fig. 7. The simulated frequency-doubled triangular waveform when the extinction ratios of two MZMs are 20 dB. (a) The bias voltage deviation ratio of MZM1 is 5%. (b) After adjusting the bias phase shift of MZM2 to 183.2°.

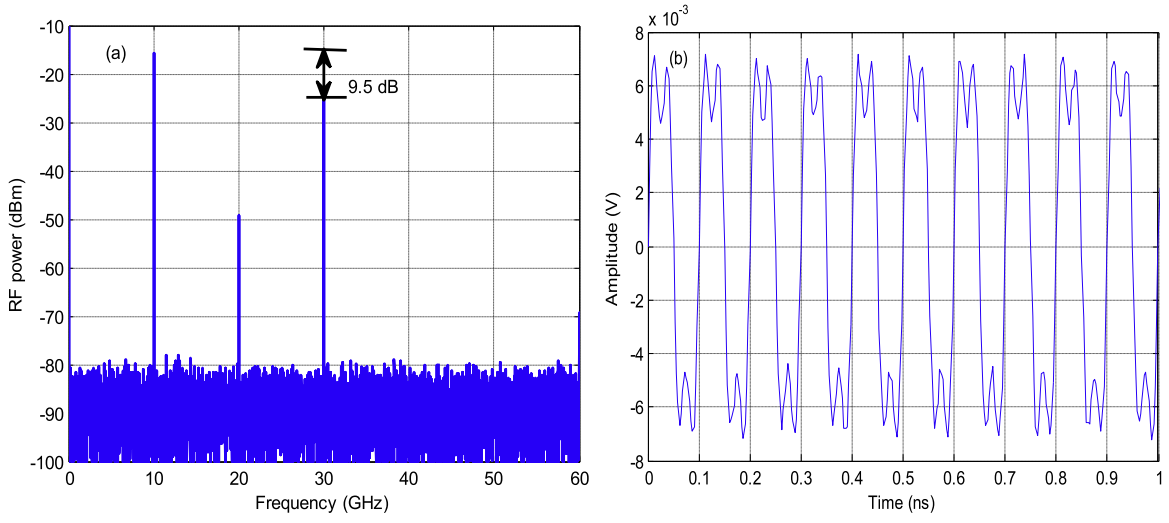

Fig. 8. Generation of frequency-doubled square waveform when the extinction ratios of two MZMs are 30 dB. (a) The simulated electrical spectrum of the 10 GHz square waveform. (b) The simulated 10 GHz square waveform.

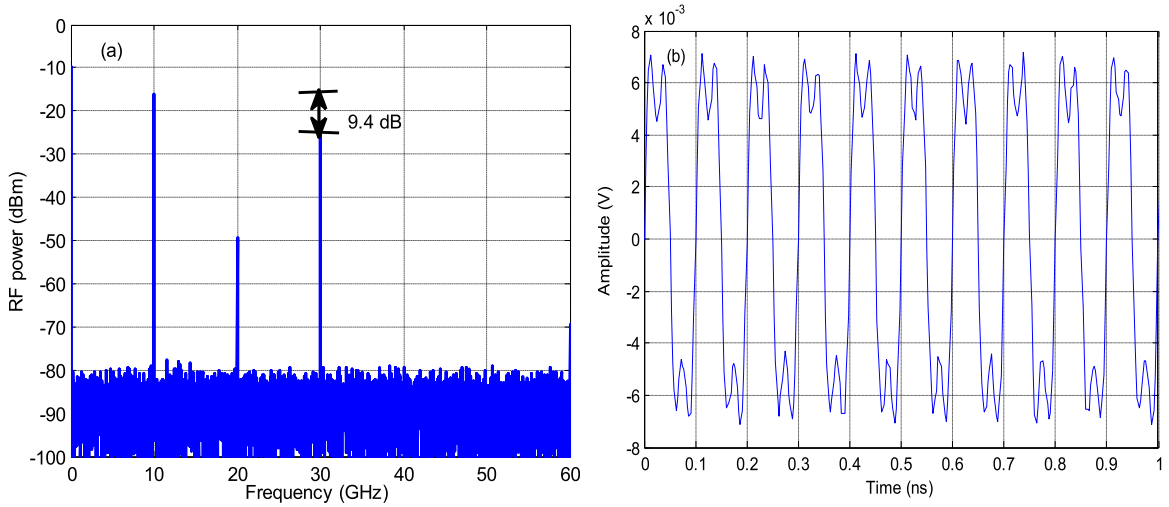

Fig. 9. Generation of frequency-doubled square waveform when the extinction ratio of MZM1 is 20 dB and the extinction ratio of MZM2 is 30 dB. (a) The simulated electrical spectrum of the 10 GHz square waveform. (b) The simulated 10 GHz square waveform.

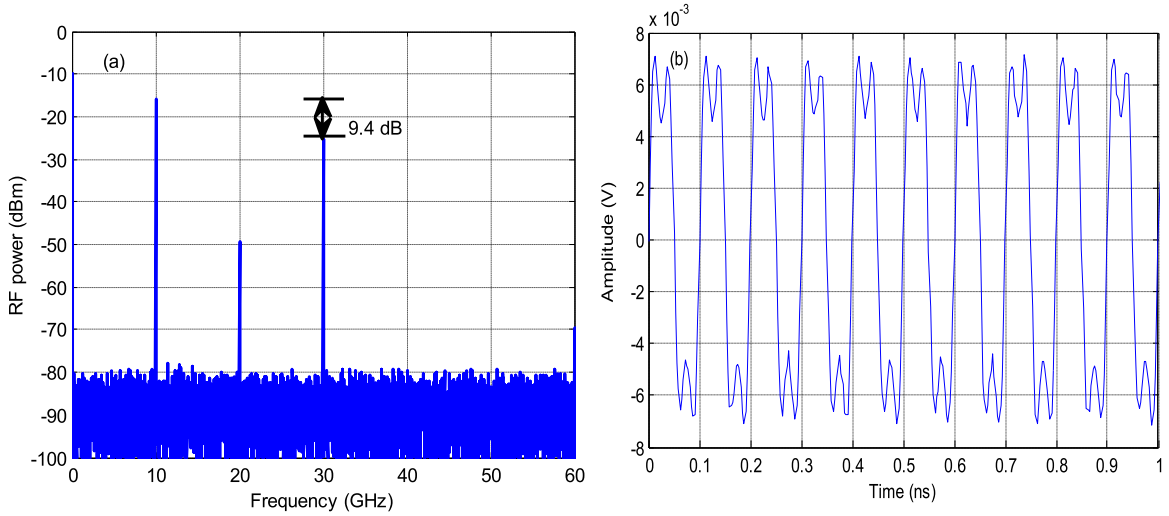

Fig. 10. Generation of frequency-doubled square waveform when the extinction ratios of two MZMs are 20 dB. (a) The simulated electrical spectrum of the 10 GHz square waveform. (b) The simulated 10 GHz square waveform.

References

[1] J.P. Yao, Photonic generation of microwave arbitrary waveforms, Opt. Commun. 284 (15) (2011) 3723–3736.

[2] Y. Park, M.H. Asghari, T.J. Ahn, J. Azana, Transform-limited picosecond pulse shaping based on temporal coherence synthesization, Opt. Express 15 (15) (2007) 9584–9599.

[3] S. Boscolo, A.I. Latkin, S.K. Turitsyn, Passive nonlinear pulse shaping in normally dispersive fiber systems, IEEE J. Quantum Electron. 44 (12) (2008) 1196–1203.

[4] A.I. Latkin, S. Boscolo, R.S. Bhamber, S.K. Turitsyn, Doubling of optical signals using triangular pulses, J. Opt. Soc. Am. B 26 (8) (2009) 1492–1496.

[5] F. Parmigiani, M. Ibsen, T.T. Ng, L. Provost, P. Petropoulos, D.J. Richardson, An efficient wavelength converter exploiting a grating-based saw-tooth pulse shaper, IEEE Photon. Technol. Lett. 20 (17) (2008) 1461–1463.

[6] C.B. Huang, D.E. Leaird, A.M. Weiner, Time-multiplexed photonically enabled radio-frequency arbitrary waveform generation with 100 ps transitions, Opt. Lett. 32 (22) (2007) 3242–3244.

[7] Z. Jiang, C.B. Huang, D.E. Leaird, A.M. Weiner, Optical arbitrary waveform processing of more than 100 spectral comb lines, Nat. Photon. 1 (8) (2007) 463–467.

[8] J. Ye, L. Yan, W. Pan, B. Luo, X. Zou, A. Yi, S. Yao, Photonic generation of triangular-shaped pulses based on frequency to time conversion, Opt. Lett. 36 (8) (2011) 1458–1460.

[9] J. Li, X. Zhang, B. Hraimel, T. Ning, Performance analysis of a photonic-assisted periodic triangular-shaped pulses generator, J. Lightw. Technol. 30 (11) (2012) 1617–1624.

[10] B. Dai, Z. Gao, X. Wang, H. Chen, N. Kataoka, N. Wada, Generation of versatile waveforms from CW light using a dual-drive Mach–Zehnder modulator and employing chromatic dispersion, J. Lightw. Technol. 31 (1) (2013) 145–151.

[11] X. Liu, W. Pan, X. Zou, D. Zheng, L. Yan, B. Luo, B. Lu, Photonic generation of triangular-shaped microwave pulses using SBS-based optical carrier processing, J. Lightw. Technol. 32 (20) (2014) 3797–3802.

[12] F. Zhang, X. Ge, S. Pan, Triangular pulse generation using a dual-parallel Mach–Zehnder modulator driven by a single-frequency radio frequency signal, Opt. Lett. 38 (21) (2013) 4491–4493.

[13] W. Li, W. Wang, N. Zhu, Photonic generation of radio-frequency waveforms based on dual-parallel Mach–Zehnder modulator, IEEE Photon. J. 6 (3) (2014) 1–8.

[14] J. Li, T. Ning, L. Pei, W. Peng, N. Jia, Q. Zhou, X. Wen, Photonic generation of triangular waveform signals by using a dual-parallel Mach–Zehnder modulator, Opt. Lett. 36 (19) (2011) 3828–3830.

[15] W. Liu, J. Yao, Photonic generation of microwave waveforms based on a polarization modulator in a Sagnac loop, J. Lightw. Technol 31 (10) (2014) 1636–1644.

[16] W. Li, W. Wang, W. Sun, W. Wang, N. Zhu, Generation of triangular waveforms based on a microwave photonic filter with negative coefficient, Opt. Express 22 (12) (2014) 14993–15001.